IEEE Access
Multidisciplinary | Rapid Review | Open Access Journal

Received August 30, 2020, accepted September 22, 2020, date of publication October 8, 2020, date of current version October 22, 2020.

Digital Object Identifier 10.1109/ACCESS.2020.3029629

Virtual Antenna Array and Multipath AOA-Delay Fingerprints Based Location for Moving Targets

ZHIGANG CHEN, (Member, IEEE), LEI WANG, AND LU CHEN
School of Information and Communications Engineering, Xi'an Jiaotong University, Xi'an 710049, China

Corresponding author: Zhigang Chen (zgchen@mail.xjtu.edu.cn)

This work was supported by the National Natural Science Foundation of China under Grant 61871317.

ABSTRACT Multipath effects are the major challenge to the accurate indoor wireless positioning technology and the most viable solutions for overcoming such multipath effects are received signal strength (RSS) or channel status information (CSI) based fingerprinting location methods. However, these fingerprinting methods are usually subject to the RSS/CSI fingerprints' high variability over space. In this paper, a novel virtual antenna array and multipath angle of arrival (AOA)-delay fingerprints based location method has been proposed. The proposed method employs 2-dimensional inverse Fourier transform on the CFRs (Channel Frequency Responses) at equi-spaced positions on a quasi-straight line moving trajectory, i.e., the CFRs of a virtual uniform linear array (VULA), to extract the equivalent multipaths' AOAs and delays as the radio fingerprints, which vary much more slowly than the RSS/CSI fingerprints in the space domain. By exploiting the geometric properties of the multipaths' AOAs and delays, a complete fingerprint database containing fingerprints of moving trajectories in different directions with each RP (reference position) as their midpoints can be constructed based on just two fingerprints of two perpendicular line trajectories with the same RP as the midpoints. Further, a two-step online fingerprinting location method is developed, the multipath delay estimates are used to narrow the scope of positioning in the first step, a modified WKNN (Weighed K-Nearest Neighbors) fingerprinting method, with the reciprocals of the fingerprints' Euclidean distances adopted as the weighting factors, is then employed on RPs in such a narrowed positioning scope to enhance the positioning accuracy. Experimental results verify that the proposed fingerprinting method outperforms the corresponding traditional RSS/CSI fingerprints based approach.

INDEX TERMS Fingerprinting localization, multipath AOA-delay fingerprints, channel frequency responses (CFRs), two-dimensional inverse Fourier transform (2D-IFT), wireless positioning.

I. INTRODUCTION

Indoor wireless positioning technology has increasingly attracted research interests [1], [2] for its wide and popular applications in the construction industry, health industry, people guidance and so on. The basic indoor positioning methods can be roughly divided into three classes, namely, time of arrival (TOA)-based methods, angle of arrival (AOA)-based methods and received signal strength (RSS) or channel status information (CSI) based methods [3]–[6]. Especially, the TOA-based methods and RSS/CSI-based methods have been extensively studied for indoor positioning in recent years, because the TOA-based methods can achieve higher positioning accuracy and the RSS/CSI-based methods can realize the location by employing the pre-existing equipment [5]–[7], thus have a low cost advantage.

However, the TOA-based location methods not only require expensive hardware to obtain the accurate TOA estimation, but are subject to the TOA estimation errors caused by the multipath effects [8], [9], which seriously limits their applications. To enhance the TOA estimation accuracy, some super-resolution TOA estimation methods, such as multiple signal classification (MUSIC) methods [9], maximum likelihood (ML) or matrix pencil (MP) methods [10], [11], have been developed, and the classical filtering schemes, such as particle filtering and Extended Kalman Filtering [12], [13], have also been employed to mitigate such multipath effects. On the other hand, such improved TOA-based location methods usually involve high computation complexity and mainly operate on the direct path's characteristics, thus can not make

The associate editor coordinating the review of this manuscript and approving it for publication was Huan Zhou.

full use of geolocation information contained in the indirect multipaths.

Meanwhile, the RSS/CSI-based methods suffer from the unstable channel variations caused by the complex multipath effects in indoor environments. In order to overcome such unstable and complex multipath effects, the most viable solutions for RSS/CSI-based positioning, named as fingerprinting positioning methods, are usually employed by comparing online RSS/CSI readings with prestored offline observations, such as the nearest neighbor (NN) methods [14], [15], the K-nearest neighbor (KNN) methods [16] and so on. Moreover, by exploiting the fine grained channel information, some improved CSI fingerprints-based positioning methods have been developed, for example, [17], [18], [18], [19] first learn the complex CSI-position dependencies based on a large offline CSI measurements-position database through compressive sensing or some classical machine learning, then use a regression scheme to estimate the position for the online RSS/CSI measurements. The methods in [21], [22] employ the probabilistic (Bayes Rule) approach to obtain the nearby reference positions' (RPs') posteriori probability, then estimate the location as the probability weighted average over the nearby RPs. Although such fingerprinting systems can achieve better performance than the conventional RSS/CSI-based methods, they are still subject to large amount of offline measurements at a large number of RPs due to the unstable RSS/CSI fingerprints, which requires laborious and complex offline database work.

Furthermore, multipath fingerprinting methods [23]–[26] employ multipaths' AOAs (angle of arrival) and/or delays, rather than the CSI or RSS, as the fingerprint extracted from the channel frequency responses (CFRs) of an antenna array, such multipath fingerprinting methods can efficiently overcome the RSS/CSI fingerprints' high variability over space since the dependencies between positions and multipaths' AOAs and delays are much more stable than RSS/CSI in the space domain, thus can achieve higher estimation accuracy. However, the applications of such multipath fingerprinting methods are limited by the requirement of a real antenna array.

In this paper, a novel virtual antenna array idea and multipath AOA-delay fingerprints based location method has been proposed. Without requiring a real antenna array, the proposed fingerprinting method employs 2-dimensional inverse Fourier transform (2D-IFT) on the CFRs at equi-spaced positions on a quasi-straight line moving trajectory, i.e., the CFRs of a virtual uniform linear array (VULA), to extract the equivalent multipaths' AOAs and delays as the radio fingerprints. Such extracted multipath AOA-delay fingerprints, on the other hand, depend on both the position of a mobile terminal (MT) and its moving direction, which leads to prohibitively huge workload of measuring the offline CFRs on line trajectories in an extra dimension of moving direction at each RP. Fortunately, the multipath AOA-delay fingerprint of a line trajectory in any direction can be expressed in terms of the radio fingerprints of two perpendicular line moving trajectories with the same mid-position. By exploiting such a geometric property of the multipaths' AOAs and delays, a complete fingerprint database, consisting of multipath AOA-delay fingerprints of line trajectories in different moving directions with each RP as the mid-position, can be constructed based on just two fingerprints of two perpendicular line moving trajectories with the same RP as their mid-positions. Furthermore, a two-step online fingerprints-based positioning method is developed by exploiting the higher multipath resolution in the 2D-IFT transformed domain, a multipath delay-based rough location is first employed to narrow the scope of positioning, a modified WKNN (Weighed K-Nearest Neighbors) fingerprinting method, with the reciprocals of the Euclidean distances between the online fingerprint and the offline fingerprints as the weighting factors, is then used on RPs in such a narrowed positioning scope to enhance the positioning accuracy.

The main contributions of this paper are as follows:

1) We present a new multipath AOA-delay fingerprint for virtual antenna array systems. Based on the CFRs at the equi-spaced positions on a quasi-straight line moving trajectory, i.e., the CFRs of a VULA, we employ 2D-IFT to extract multipaths' AOAs and delays as the fingerprints, which vary much more slowly than the traditional CSI/RSS fingerprints across the space dimension.

2) By exploiting the geometric property of the multipaths' AOAs and delays, we can construct a complete fingerprint database containing fingerprints of moving trajectories with each RP as the midpoints in different directions based on just two fingerprints of two perpendicular line moving trajectories with the same RP as their midpoints.

3) We propose a two-step fingerprinting location method. The proposed method employs the multipath delay-based location scheme to narrow the scope of positioning, then implements a modified WKNN fingerprinting method based on the Euclidean distances between the online fingerprint and the offline fingerprints to enhance the positioning accuracy.

4) Experimental results demonstrate that the proposed fingerprinting method outperforms the corresponding traditional RSS/CSI fingerprints based approach.

The rest of this paper is organized as follows. In Section II, a virtual antenna array system model is presented and the multipath AOA-delay fingerprint is defined. We develop a novel scheme for constructing the offline radio fingerprint database and propose a novel two-step fingerprinting location method based on the properties of multipath AOA-delay fingerprints in Section III. The experimental validation of the proposed method is presented in Section IV. We also discuss some practical problems about the proposed method in section V. Finally, conclusions are drawn in Section VI.

II. SYSTEM MODEL

A. VIRTUAL ANTENNA ARRAY SYSTEM MODEL

For ease of description, we consider an OFDM WLAN system with K access points (APs) and a MT. Suppose that the MT moves in a quasi-straight line in a horizontal plane

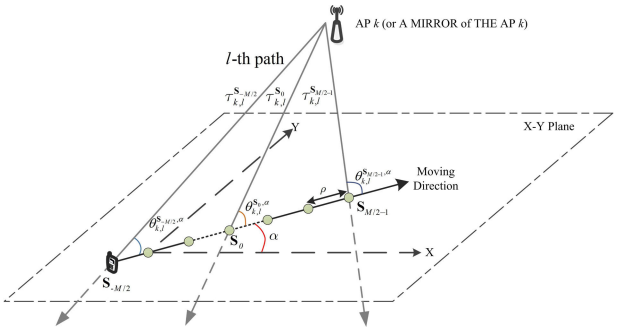

FIGURE 1. Illustration of the l-th multipath's AOAs and delays at equi-spaced positions on the line trajectory.

during a short time period, such as a period of 1 second or 0.5 seconds, which is usually the case as pedestrians walk in indoor environments. For simplicity, the horizontal plane can be described as an X-Y plane and the angle of the MT's moving direction relative to the X-axis is denoted as α. When the MT's acceleration, which can be measured by built-in accelerometers or inertial sensors in the MT [27], [28], is smaller than a chosen threshold, the MT can be assumed to make uniform linear motion with imprecisely estimated velocity due to the unknown accumulated error of built-in sensors. By simply taking positions at M equi-interval moments or taking positions where multipaths' phases vary linearly during such a short period of relatively small acceleration (see section V.B for details), we can obtain M equi-spaced positions $\{S_m = (x_m, y_m)\}_{m=-M/2}^{M/2-1}$ with position spacing of ρ, which is also imprecisely estimated due to the rough estimation of moving distance in such a short period, on the quasi-straight line moving trajectory of the MT.

The CFRs at such M equi-spaced positions can be regarded as the CFRs of a virtual uniform linear array (VULA) at its central position S_0. The channel impulse response (CIR) between the MT at the m-th position S_m and the k-th AP is given by [29]

$$h_k(t, m) = \sum_{l=1}^{L_k} \zeta_{k,l}^{S_m,\alpha} a\left(\theta_{k,l}^{S_m,\alpha}\right) \delta\left(t - \tau_{k,l}^{S_m,\alpha}\right) \quad m = -M/2, \cdots, (M-1)/2 \tag{1}$$

where L_k is the number of distinct propagation paths from the k-th AP to the MT at the m-th position S_m, $\zeta_{k,l}^{S_m,\alpha}$, $\tau_{k,l}^{S_m,\alpha}$ and $\theta_{k,l}^{S_m,\alpha}$ denote the complex gain, the propagation time delay and the AOA relative to the moving trajectory of the l-th path in the channel between the MT at the m-th position S_m and the k-th AP, respectively, which are also shown in Fig. 1. $a\left(\theta_{k,l}^{S_m,\alpha}\right) = e^{-j2\pi f \tau\left(\theta_{k,l}^{S_m,\alpha}\right)}$ is the array response of the m-th virtual antenna to the l-th path. Considering the path gain $\zeta_{k,l}^{S_m,\alpha}$ and the path delay $\tau_{k,l}^{S_m,\alpha}$ are irrelevant to the moving direction, the superscript α of $\zeta_{k,l}^{S_m,\alpha}$ and $\tau_{k,l}^{S_m,\alpha}$ is omitted as $\zeta_{k,l}^{S_m}$ and $\tau_{k,l}^{S_m}$ in the following.

Therefore, the estimated channel frequency response (CFR) at the n-th subcarrier and the m-th position can be expressed as:

$$H_k(m, n) = \sum_{l=1}^{L_k} \zeta_{k,l}^{S_m} \exp(-j2\pi f_c \tau_{k,l}^{S_m}) \exp(-j2\pi \Delta f n \tau_{k,l}^{S_m}) + W_k(m, n) \tag{2}$$

where f_c and Δf represent the carrier frequency and the OFDM subcarrier spacing, respectively. $W_k(m, n) \sim \mathcal{CN}(0, \sigma^2)$ is the additive white Gaussian noise (AWGN).

According to the cosine-theorem, the path delay $\tau_{k,l}^{S_m}$ can be expressed as

$$\begin{aligned}\tau_{k,l}^{S_m} &= \frac{1}{c}\sqrt{(m\rho)^2 + \left(\tau_{k,l}^{S_0} c\right)^2 + 2m\rho\tau_{k,l}^{S_0} c\cos\theta_{k,l}^{S_0,\alpha}} \\ &\approx \frac{1}{c}\left(\tau_{k,l}^{S_0} c + m\rho\cos\theta_{k,l}^{S_0,\alpha}\right)\end{aligned} \tag{3}$$

where c is the speed of light, the approximation holds for $\frac{M\rho}{2c\tau_{k,l}^{S_0}} \ll 1$, i.e. the size of VULA is greatly smaller than the path distance.

By substituting (3) into (2), (2) can be further expressed as:

$$\begin{aligned}&H_k(m, n) \\ &\approx \sum_{l=1}^{L} \zeta_{k,l}^{S_m} \exp(-j2\pi f_c(\tau_{k,l}^{S_0} + \frac{m\rho\cos\theta_{k,l}^{S_0,\alpha}}{c})) \\ &\quad \cdot \exp(-j2\pi\Delta f n\tau_{k,l}^{S_0}) + W_k(m, n) \\ &\approx \sum_{l=1}^{L} \acute{\zeta}_{k,l}^{S_m} \exp(-j2\pi f_c \frac{m\rho\cos\theta_{k,l}^{S_0,\alpha}}{c}) \cdot \exp(-j2\pi\Delta f n\tau_{k,l}^{S_0}) \\ &\quad + W_k(m, n)\end{aligned} \tag{4}$$

where the first approximation holds due to

$$\exp(-j2\pi\Delta f n\frac{m\rho\cos\theta_{k,l}^{S_0,\alpha}}{c}) \approx 1$$

in narrowband systems, $\acute{\zeta}_{k,l}^{S_m} = \zeta_{k,l}^{S_m} e^{-jf_c\tau_{k,l}^{S_0}}$ is approximately constant for cases of $\frac{M\rho}{2c\tau_{k,l}} \ll 1$ and can be approximated as $\acute{\zeta}_{k,l}^{S_m} \approx \acute{\zeta}_{k,l}^{S_0} = \zeta_{k,l}^{S_0} e^{-jf_c\tau_{k,l}^{S_0}}$.

B. MULTIPATHS' AOAs AND DELAYS BASED FINGERPRINT

By implementing a two-dimensional discrete IFT across the space and frequency dimensions on the CFRs in (4), we have

$$\begin{aligned}&\tilde{H}_k(u, v) \\ &= \frac{1}{\sqrt{MN}} \sum_{n=1}^{N}\sum_{m=1}^{M} \{H_k(m, n)\ \exp(j2\pi um/M)\} \\ &\quad \cdot \exp(j2\pi vn/N) + \tilde{W}_k(m, n) \\ &= \frac{1}{\sqrt{MN}} \sum_{l=1}^{L} \acute{\zeta}_{k,l}^{S_0} \frac{\sin(\pi(b_{k,l}^{S_0,\alpha} - u))}{\sin(\pi(b_{k,l}^{S_0,\alpha} - u)/M)} \frac{\sin(\pi(\bar{\tau}_{k,l}^{S_0} - v))}{\sin(\pi(\bar{\tau}_{k,l}^{S_0} - v)/N)} \\ &\quad \cdot \exp(-j\pi(\frac{(M-1)(b_{k,l}^{S_0,\alpha} - u)}{M} + \frac{(N-1)(\bar{\tau}_{k,l}^{S_0} - v)}{N})) \\ &\quad + \tilde{W}_k(m, n)\end{aligned} \tag{5}$$

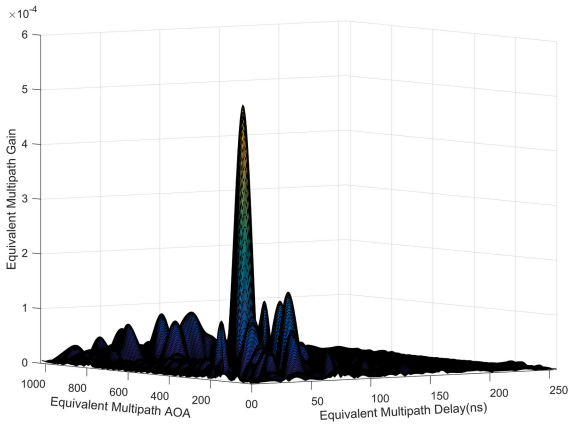

FIGURE 2. Experimental results of multipath resolution in a VULA system in an indoor environment.

with

$$b_{k,l}^{S_0,\alpha} = M\rho f_c \cos\theta_{k,l}^{S_0,\alpha}/c$$
$$\mathcal{T}_{k,l}^{S_0} = N\Delta f \tau_{k,l}^{S_0} \tag{6}$$

where $\acute{\zeta}_{k,l}^{S_0}$, $b_{k,l}^{S_0,\alpha}$ and $\mathcal{T}_{k,l}^{S_0}$ represent the equivalent gain, the equivalent AOA and the normalized equivalent time delay of the l-th path, respectively.

From (5), if the space 'bandwidth', i.e. the VULA size $M\rho$, is sufficiently large, the multipaths' equivalent AOAs and the equivalent time delays can be estimated with less interference by searching for the L_k peaks of the CFRs $\left\{(\hat{b}_{k,l_k}^{S_0,\alpha}, \hat{\mathcal{T}}_{k,l_k}^{S_0})\right\}_{l_k=1}^{L_k}$ in the 2D-IFT transformed domain, i.e., the higher multipath resolution can be achieved in the 2D-IFT transformed domain than in the traditional 1-dimensional delay domain even if the system bandwidth $B = N\Delta f$ is limited, which is shown in Fig. 2. Moreover, the AOAs and the time delays of multipaths vary slowly and stably in the space domain, which means that such multipath parameters are much more robust than the RSS or CSI in the space domain.

In order to exploit the abovementioned multipaths' characteristics in the AOA-delay domain, we define the radio fingerprint between the K APs and the MT on the trajectory in a moving angle α in terms of the estimated equivalent AOAs and normalized time delays of the distinct multipaths as

$$\begin{aligned}\mathcal{F}^{S_0,\alpha} &= \left\{\mathcal{F}_1^{S_0,\alpha}, \cdots, \mathcal{F}_K^{S_0,\alpha}\right\} \\ &= \left\{\left\{(\hat{b}_{1,l_1}^{S_0,\alpha}, \hat{\mathcal{T}}_{1,l_1}^{S_0})\right\}_{l_1=1}^{L_1}, \cdots, \left\{(\hat{b}_{K,l_K}^{S_0,\alpha}, \hat{\mathcal{T}}_{K,l_K}^{S_0})\right\}_{l_K=1}^{L_K}\right\}\end{aligned} \tag{7}$$

This radio fingerprint is relevant to the central position S_0 and the direction α of the trajectory, hence it will be simply called as the fingerprint at the central position S_0 in a moving angle α in the following. Considering that the number of the distinct multipaths in the channels is sufficiently large, it is unique for each combination of a position and a moving direction.

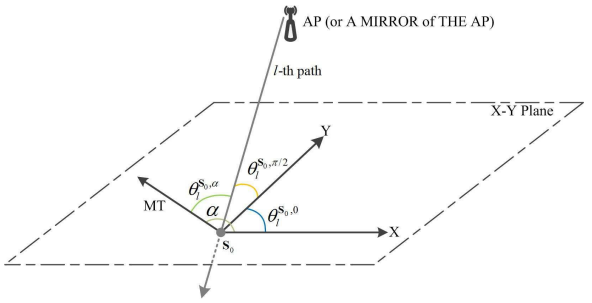

FIGURE 3. The relationship of the l-th multipath's AOAs relative to different moving directions.

III. MULTIPATH AOA-DELAY FINGERPRINTS-BASED POSITIONING ALGORITHM

In this section, the properties of the radio fingerprint defined in (7) will be first analyzed. Based on these properties, a novel scheme for constructing the offline radio fingerprint database will be then developed, and a novel two-step fingerprinting location method will be proposed finally.

A. PROPERTIES OF THE AOA-DELAY FINGERPRINT

1) THE RELATIONSHIP OF FINGERPRINTS OF LINE TRAJECTORIES IN DIFFERENT DIRECTIONS WITH THE SAME MID-POSITION

Suppose that there are three line moving trajectories respectively in X-axis direction, Y-axis direction and the moving direction of angle α with the same mid-position S_0, which are shown in Fig. 3. The equivalent AOAs and normalized time delays of the l-th path in CFRs on these three line moving trajectories are denoted as $(\hat{b}_l^{S_0,0} = M\rho f_c \cos\theta_l^{S_0,0}/c, \hat{\mathcal{T}}_l^{S_0,0} = N\Delta f \tau_l^{S_0})$, $(\hat{b}_l^{S_0,\pi/2} = M\rho f_c \cos\theta_l^{S_0,\pi/2}/c, \hat{\mathcal{T}}_l^{S_0,\pi/2} = N\Delta f \tau_l^{S_0})$ and $(\hat{b}_l^{S_0,\alpha} = M\rho f_c \cos\theta_l^{S_0,\alpha}/c, \hat{\mathcal{T}}_l^{S_0,\alpha} = N\Delta f \tau_l^{S_0})$.

The equivalent normalized time delay of the l-th path in CFRs on these three line moving trajectories are the same since the path delay $\tau_l^{S_0}$ are only relevant to the position. According to the cosine theorem of the trihedral angle, it can be obtained that

$$cos\theta_l^{S_0,\alpha} = cos\alpha \cdot cos\theta_l^{S_0,0} + sin\alpha \cdot cos\theta_l^{S_0,\pi/2} \tag{8}$$

Thus the equivalent AOA and normalized time delay of the l-th path in CFRs on the line moving trajectory with the same mid-position S_0 in a moving angle α can be expressed as

$$\left\{\hat{b}_l^{S_0,\alpha} = cos\alpha \cdot \hat{b}_l^{S_0,0} + sin\alpha \cdot \hat{b}_l^{S_0,\pi/2}, \quad \hat{\mathcal{T}}_l^{S_0,\alpha} = \hat{\mathcal{T}}_l^{S_0,\pi/2} = \hat{\mathcal{T}}_l^{S_0,0}\right\} \tag{9}$$

Therefore, the radio fingerprint of a line trajectory in any direction can be expressed in terms of the radio fingerprints of two perpendicular line moving trajectories with the same mid-position.

2) THE EUCLIDEAN DISTANCE BETWEEN FINGERPRINTS OF TWO PARALLEL LINE TRAJECTORIES

Without losing generality, suppose that there are two line trajectories in the X-axis direction with different mid-positions,

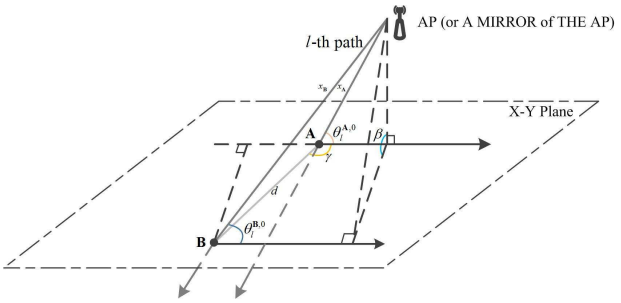

FIGURE 4. The geometric relationship between the *l*-th multipath and two parallel line trajectories at different positions.

position A and B, which are shown in Fig. 4. The equivalent AOAs and normalized time delays of the l-th path in the CFRs on these two trajectories are $(\hat{b}_l^{A,0} = M\rho f_c \cos\theta_l^{A,0}/c, \hat{\mathcal{T}}_l^A = N\Delta f \tau_l^A)$ and $(\hat{b}_l^{B,0} = M\rho f_c \cos\theta_l^{B,0}/c, \hat{\mathcal{T}}_l^B = N\Delta f \tau_l^B)$, respectively.

Denote the distance between position A and position B as d and the lengths of the l-th path at position A and position B as x_A and x_B. And denote the angle between the moving direction and the line AB as γ and the angle between the horizontal plane and the plane containing the l-th path at position A and a line crossing position A in the X-axis direction as β. Then it can be proved (See Appendix for the derivation) that

$$\begin{aligned}
&\hat{b}_l^{A,0} - \hat{b}_l^{B,0} \\
&\approx \frac{d\left(\cos\gamma - (\cos\theta_l^{A,0}\cos\gamma - \sin\theta_l^{A,0}\sin\gamma\cos\beta)\cos\theta_l^{A,0}\right)M\rho f_c}{x_A \cdot c} \\
&\hat{\mathcal{T}}_l^A - \hat{\mathcal{T}}_l^B = N\Delta f d\left(\cos\theta_l^{A,0}\cos\gamma - \sin\theta_l^{A,0}\sin\gamma\cos\beta\right)/c
\end{aligned} \tag{10}$$

in cases of $d \ll x_A$.

It is obvious from (10) that the Euclidean distance between the equivalent AOAs and normalized time delays of the l-th path at position A and B is proportional to the distance between position A and position B if $d \ll x_A$ holds.

As an averaged quantity over multipaths, the Euclidean distance between fingerprints of two parallel trajectories with their mid-positions in a relatively small range is proportional to the distance between these two mid-positions.

B. CONSTRUCTION OF THE AOA-DELAY FINGERPRINT DATABASE

From (7), the proposed AOA-delay fingerprint in a VULA system is unique for each combination of the trajectory's mid-position and the moving direction, hence the fingerprints at each RP in different moving directions should be recorded in the offline radio 'map', which means prohibitively huge workload of measuring the offline CFRs on trajectories in an extra dimension of moving direction at each RP.

Fortunately, the radio fingerprint of a line trajectory in any direction can be expressed in terms of the radio fingerprints of two perpendicular line trajectories with the same mid-position by using the relationship of fingerprints of line trajectories in different directions in (9). Therefore, only the AOA-delay fingerprints of moving trajectories with each RP as their mid-position in the X-axis direction and the Y-axis direction need to be obtained through field measurements, which are expressed as

$$\begin{aligned}
\mathcal{F}^{R_p,0} &= \left\{\mathcal{F}_1^{R_p,0}, \cdots, \mathcal{F}_K^{R_p,0}\right\} \\
&= \left(\left\{(\hat{b}_{1,l_1}^{R_p,0}, \hat{\mathcal{T}}_{1,l_1}^{R_p,0})\right\}_{l_1=1}^{L_1^p}, \cdots, \left\{(\hat{b}_{K,l_K}^{R_p,0}, \hat{\mathcal{T}}_{K,l_K}^{R_p,0})\right\}_{l_K=1}^{L_K^p}\right)
\end{aligned} \tag{11}$$

and

$$\begin{aligned}
&\mathcal{F}^{R_p,\frac{\pi}{2}} \\
&= \left\{\mathcal{F}_1^{R_p,\frac{\pi}{2}}, \cdots, \mathcal{F}_K^{R_p,\frac{\pi}{2}}\right\} \\
&= \left(\left\{(\hat{b}_{1,l_1}^{R_p,\frac{\pi}{2}}, \hat{\mathcal{T}}_{1,l_1}^{R_p,\frac{\pi}{2}})\right\}_{l_1=1}^{L_1^p}, \cdots, \left\{(\hat{b}_{K,l_K}^{R_p,\frac{\pi}{2}}, \hat{\mathcal{T}}_{K,l_K}^{R_p,\frac{\pi}{2}})\right\}_{l_K=1}^{L_K^p}\right),
\end{aligned} \tag{12}$$

respectively, where R_p denotes the p-th RP.

It is worth mentioning that only the equivalent AOAs and the normalized time delays of the main paths, with their equivalent gains greater than a chosen threshold, are used as the components of radio fingerprints to mitigate the noise and interference effects. For convenience, the components of radio fingerprints between each AP and the MT are arranged in an ascending order of multipath delay. Moreover, by using the property that each multipath's equivalent normalized time delay and gain for the trajectory with the p-th RP, R_p, as its midpoint in the X-axis direction is same or almost same as the multipath's counterparts for the trajectory with the same midpoint R_p in the Y-axis direction, the components in the fingerprints $\mathcal{F}^{R_p,0}$ and $\mathcal{F}^{R_p,\pi/2}$ can be paired according to the multipath order. In other words, both the lth component $(\hat{b}_{k,l}^{(R_p,0)}, \hat{\mathcal{T}}_{k,l}^{R_p,0})$ in $\mathcal{F}_k^{R_p,0}$ and the lth component $(\hat{b}_{k,l}^{R_p,\pi/2}, \hat{\mathcal{T}}_{k,l}^{R_p,\pi/2})$ in $\mathcal{F}_k^{R_p,\pi/2}$ correspond to the same path, i.e. the l-th multipath.

From (9), the fingerprint of the moving trajectory in the angle α_p relative to the X-axis with the p-th RP as its midpoint can be derived as

$$\begin{aligned}
&\mathcal{F}^{R_p,\alpha_p} \\
&= \left\{\mathcal{F}_1^{R_p,\alpha_p}, \cdots, \mathcal{F}_K^{R_p,\alpha_p}\right\} \\
&= \left(\left\{(\hat{b}_{1,l_1}^{R_p,\alpha_p}, \hat{\mathcal{T}}_{1,l_1}^{R_p,\alpha_p})\right\}_{l_1=1}^{L_1^p}, \cdots, \left\{(\hat{b}_{K,l_K}^{R_p,\alpha_p}, \hat{\mathcal{T}}_{K,l_K}^{R_p,\alpha_p})\right\}_{l_K=1}^{L_K^p}\right)
\end{aligned} \tag{13}$$

with

$$\begin{aligned}
\hat{b}_{k,l_k}^{R_p,\alpha_p} &= \cos\alpha_p \hat{b}_{k,l_k}^{R_p,0} + \sin\alpha_p \hat{b}_{k,l_k}^{R_p,\pi/2} \\
\hat{\mathcal{T}}_{k,l_k}^{R_p,\alpha_p} &= \left(\hat{\mathcal{T}}_{k,l_k}^{R_p,0} + \hat{\mathcal{T}}_{k,l_k}^{R_p,\pi/2}\right)/2
\end{aligned} \tag{14}$$

Therefore, the fingerprint database for P RPs and Q discretized moving directions, i.e. $\{\alpha_p = 2\pi q/Q\}_{q=0}^{Q-1}$, relative

to the X-axis is expressed as

$$\Phi = \left\{ \{\mathcal{F}^{R_p, 2\pi \cdot q/Q}\}_{q=0}^{Q-1} \right\}_{p=1}^{P} \tag{15}$$

The pseudocode for constructing the AOA-Delay fingerprint database is given in Algorithm 1.

Algorithm 1 Constructing the AOA-Delay Fingerprint Map

Input: CFRs $\{H_k(m,n)\}_{m=1,n=1}^{M,N}$ at N subcarriers and M equi-spaced positions on the quasi-straight line moving trajecory with each RP as its mid-position in the X-axis direction and Y-axis direction, respectively;

Output: The AOA-delay fingerprint database $\Phi = \left\{ \{\mathcal{F}^{R_p, 2\pi \cdot q/Q}\}_{q=0}^{Q-1} \right\}_{p=1}^{P}$;

1: **for** each R_p, $p \in [1, P]$ **do**
2: **for** each AP $k \in [1, K]$ **do**
3: // Obtain AOA-delay fingerprints at R_p in the X-axis direction and Y-axis direction
4: Compute the AOA-delay fingerprint at R_p in the X-axis direction and Y-axis direction, $\mathcal{F}^{R_p,\alpha_p=0} = \left\{ (\hat{b}_{k,l_k}^{R_p,0}, \hat{\mathcal{T}}_{k,l_k}^{R_p,0}) \right\}_{l_k=1}^{L_k^p}$ and $\mathcal{F}^{R_p,\alpha_p=\frac{\pi}{2}} = \left\{ (\hat{b}_{k,l_k}^{R_p,\frac{\pi}{2}}, \hat{\mathcal{T}}_{k,l_k}^{R_p,\frac{\pi}{2}}) \right\}_{l_k=1}^{L_k^p}$ by implementing 2D-IFT on the collected CFRs in the X-axis direction and Y-axis direction, respectively;
5: // Constructing AOA-delay fingerprints at R_p in Q discretized directions
6: **for** each direction $\alpha_p = 2\pi q/Q$, $q \in [1, Q]$ **do**
$\hat{b}_{k,l_k}^{R_p,\alpha_p} = \cos\alpha_p \hat{b}_{k,l_k}^{R_p,0} + \sin\alpha_p \hat{b}_{k,l_k}^{R_p,\pi/2}$
$\hat{\mathcal{T}}_{k,l_k}^{R_p,\alpha_p} = \left(\hat{\mathcal{T}}_{k,l_k}^{R_p,0} + \hat{\mathcal{T}}_{k,l_k}^{R_p,\pi/2} \right)/2$
$\mathcal{F}_k^{R_p,\alpha_p} = \left\{ (\hat{b}_{k,l_1}^{R_p,\alpha_p}, \hat{\mathcal{T}}_{k,l_k}^{R_p,\alpha_p}) \right\}_{l_k=1}^{L_k^p}$;
7: **end for**
8: **end for**
9: $\{\mathcal{F}^{R_p,\frac{2q\pi}{Q}}\}_{q=0}^{Q-1} = \left\{ \mathcal{F}_1^{R_p,\frac{2q\pi}{Q}}, \cdots, \mathcal{F}_K^{R_p,\frac{2q\pi}{Q}} \right\}_{q=0}^{Q-1}$;
10: **end for**

C. AOA-DELAY FINGERPRINTS BASED POSITIONING METHOD

Based on the offline AOA-delay fingerprint database, a two-step online fingerprinting location method is developed in this section. By exploiting the higher multipath resolution in the 2D-IFT transformed domain, the multipath delay estimates based rough location is employed to narrow the scope of positioning for the MT in the first step. Further, a modified WKNN fingerprinting method will be used in such a narrowed spatial scope to enhance the positioning accuracy.

1) NARROWING THE SCOPE OF POSITIONING

Since not only the multipaths' characteristics in the frequency domain but also the ones in the space domain have been exploited in a virtual antenna array system, the 2D-IFT in the space-frequency domain can achieve higher multipath resolution than the conventional frequency domain IFFT, thus the multipaths' delays can be estimated with higher accuracy in this 2D transformed domain. Moreover, the multipaths' delays are irrelevant to the online VULA element spacing from (6). Hence the estimated direct path delays are first used to narrow the scope of positioning for the MT as follows.

Assume that the online fingerprint is estimated from the online CFRs as

$$\begin{aligned} \tilde{\mathcal{F}}^{O,\tilde{\alpha}} &= \left\{ \tilde{\mathcal{F}}_1^{O,\tilde{\alpha}}, \cdots, \tilde{\mathcal{F}}_K^{O,\tilde{\alpha}} \right\} \\ &= \left\{ \left\{ (\hat{b}_{1,l_1}^{O,\tilde{\alpha}}, \hat{\mathcal{T}}_{1,l_1}^{O}) \right\}_{l_1=1}^{\tilde{L}_1}, \cdots, \left\{ (\hat{b}_{K,l_K}^{O,\tilde{\alpha}}, \hat{\mathcal{T}}_{K,l_K}^{O}) \right\}_{l_K=1}^{\tilde{L}_K} \right\} \end{aligned} \tag{16}$$

where $\hat{\mathcal{T}}_{k,l}^{O} = N\Delta f \tau_{k,l}^{O}$ and $\hat{b}_{k,l}^{O,\tilde{\alpha}} = M\tilde{\rho} f_c \cos\theta_{k,l}^{O,\tilde{\alpha}}/c$ with $\tilde{\rho}$, O and $\tilde{\alpha}$ denoting the online VULA element spacing, the MT's online position and the moving direction, respectively.

The equivalent delay of the direct path from the k-th AP to the MT is obtained as the minimum equivalent multipath delay component in the fingerprint. Without loss of generality, let the first component of all the fingerprints correspond to the direct path, i.e.

$$\begin{aligned} \hat{\mathcal{T}}_{k,1}^{O} &\triangleq \min \left\{ \{\hat{\mathcal{T}}_{k,l_k}^{O}\}_{l_k=1}^{L_k} \right\} \\ \hat{\mathcal{T}}_{k,1}^{R_p} &\triangleq \min \left\{ \{\hat{\mathcal{T}}_{k,l_k}^{R_p}\}_{l_k=1}^{L_k} \right\} \end{aligned} \tag{17}$$

Then the nearby RPs of the MT can be chosen as the RPs satisfying

$$\max \left(\left| \hat{\mathcal{T}}_{k=1,1}^{R_p} - \hat{\mathcal{T}}_{k=1,1}^{O} \right|, \cdots, \left| \hat{\mathcal{T}}_{K,1}^{R_p} - \hat{\mathcal{T}}_{K,1}^{O} \right| \right) \le T_b \quad p = 1, 2, \cdots, P \tag{18}$$

where T_b is a chosen delay difference threshold.

Define the set of fingerprints of the nearby RPs as

$$\Phi' = \left\{ \{\mathcal{F}^{(R_{\mathcal{I}(p')}, 2\pi \cdot q/Q)}\}_{q=0}^{Q-1} \right\}_{p'=1}^{P'} \tag{19}$$

where $\mathcal{I}$ and P' denote the set of the nearby RPs' indexes and its size, respectively.

2) WKNN FINGERPRINTING BASED LOCATION

In this step, the Euclidean distances between the online fingerprint and the offline fingerprints at the nearby RPs are first obtained as the similarity metric between the MT's position and its nearby RPs, then a modified WKNN positioning algorithm [23] is applied to estimate the location of MT based on this similarity metric.

The online fingerprint is dependent on not only the MT's position but also the MT's moving direction α and the online mean VULA element-spacing from (6). The offline mean VULA element-spacing is accurately known since the offline moving trajectory is deliberately chosen, while the online mean element-spacing is imprecisely estimated due to the

rough estimation of online moving distance. Without losing generality, we model the imprecisely estimated online mean VULA element-spacing as $\tilde{\rho} = e \cdot \rho$ with ρ and e denoting the offline mean VULA element-spacing and the scaling factor of the online mean element-spacing in a known range $\mathbb{E}$, respectively.

Given the online position O and the online moving direction $\tilde{\alpha}$, the online equivalent multipaths' AOA estimates for $\tilde{\rho} = e \cdot \rho$ can be expressed as the corresponding offline equivalent multipaths' AOAs multiplied by the scaling factor of the online VULA element-spacing from (6), hence the equivalent online multipath AOA-delay fingerprint with the offline mean VULA element-spacing can be expressed as

$$\hat{\mathcal{F}}^{O,\tilde{\alpha},e} = \left\{ \left\{ (\frac{1}{e}\hat{b}^{O,\tilde{\alpha}}_{1,l_1}, \hat{\mathcal{T}}^{O}_{1,l_1}) \right\}_{l_1=1}^{\tilde{L}_1}, \cdots, \left\{ (\frac{1}{e}\hat{b}^{O,\tilde{\alpha}}_{K,l_K}, \hat{\mathcal{T}}^{O}_{K,l_K}) \right\}_{l_K=1}^{\tilde{L}_K} \right\} \tag{20}$$

By exploiting the slowly space-varying property of multipaths' AOAs and delays and the uniqueness of the multipath AOA-delay fingerprint for each combination of the position and the moving direction, it can be derived that the Euclidean distance between the online fingerprint and the fingerprints of the p'-th nearby RP achieves its minimum value at $\alpha_{p'} = \tilde{\alpha}$ and $\tilde{\rho} = \rho$. Hence, the minimum Euclidean distance between the online fingerprint and the fingerprints of the p'-th nearby RP with respect to $\alpha_{p'}$ and $\tilde{\rho}$ can be obtained as

$$\delta_{p'} \triangleq \min_{q=1,\cdots,Q;e\in\mathbb{E}} \|\hat{\mathcal{F}}^{O,\tilde{\alpha},e} - \mathcal{F}^{(R_{\mathcal{I}(p')},2\pi\cdot q/Q)}\| \quad p' = 1, 2, \cdots, P' \tag{21}$$

where $\|\cdot\|$ represents Euclidean distance operation. As a result, $\delta_{p'}$ represents the Euclidean distance between the online fingerprint and the p'-th nearby RP's fingerprint for the same moving direction and the same VULA element spacing, i.e., $\alpha_{p'} = \tilde{\alpha}$ and $\tilde{\rho} = \rho$.

Considering that the MT is surrounded by the nearby RPs in a narrowed positioning scope, it can be proved by using analytic geometry that the location of MT can be approximately expressed as the weighted average of the nearby RPs, with the weighting factor of each nearby RP chosen as the reciprocal of the spatial distance between the nearby RP and the MT. According to the geometric property of the AOA-delay fingerprint in section III.A.2), i.e., the Euclidean distances between the online fingerprint and the nearby RPs' fingerprints in the same moving direction are proportional to the spatial distances between the MT and the nearby RPs, the WKNN positioning algorithm [23] can be applied to estimate the location of the MT, but the weighting factor of each nearby RP is modified proportional to the reciprocal of the Euclidean distance between the online fingerprint and the nearby RP's fingerprint.

Therefore, the MT's position O can be estimated as

$$\hat{O} = \sum_{p'=1}^{P'} \omega_{p'} R_{p'} \tag{22}$$

with the weighting factor

$$\omega_{p'} = \frac{1/\delta_{p'}}{\sum_{p'=1}^{P'} 1/\delta_{p'}}. \tag{23}$$

The pseudocode for the proposed AOA-Delay fingerprints based positioning method is given in Algorithm 2.

Algorithm 2 AoA-Delay Fingerprints Based Positioning

Input: The AOA-delay fingerprint map and the online CFRs $\{\tilde{H}_k(m,n)\}_{k=1,m=1,n=1}^{K,M,N}$ between the MT and the K APs at N subcarriers and M equi-spaced positions on the moving trajectory;

Output: the estimated MT's location $\hat{O}$;

1: Extract the online AOA-delay fingerprint $\tilde{\mathcal{F}}^{O,\tilde{\alpha}} = \left\{ \tilde{\mathcal{F}}^{O,\tilde{\alpha}}_1, \cdots, \tilde{\mathcal{F}}^{O,\tilde{\alpha}}_K \right\}$ from the online CFRs through 2D-IFT;

2: Select the nearby RPs with their minimum path delays in fingerprints satisfying $\max\left(\left| \hat{\mathcal{T}}^{R_p}_{k=1,1} - \hat{\mathcal{T}}^{O}_{k=1,1} \right|, \cdots, \left| \hat{\mathcal{T}}^{R_p}_{K,1} - \hat{\mathcal{T}}^{O}_{K,1} \right| \right) \le T_b$ $p = 1, 2, \cdots, P$;

3: // Compute the Euclidean distance for each nearby RP

4: **for** each nearby RP $p' \in [1, P']$ **do** $\delta_{p'} \triangleq \min_{q=1,\cdots,Q;e\in\mathbb{E}} \|\hat{\mathcal{F}}^{O,\tilde{\alpha},e} - \mathcal{F}^{(R_{\mathcal{I}(p')},2\pi\cdot q/Q)}\|$;

5: **end for**

6: Estimate the online position by WKNN $\hat{O} = \sum_{p'=1}^{P'} \omega_{p'} R_{p'}$ with $\omega_{p'} = \frac{1/\delta_{p'}}{\sum_{p'=1}^{P'} 1/\delta_{p'}}$;

IV. EXPERIMENT VALIDATION

A. EXPERIMENT METHODOLOGY

In this section, some experimental results are presented to evaluate the performance of the proposed algorithm and compare it with the typical fingerprinting location algorithms: the FIFS algorithm [21], the CSI-MIMO algorithm [22] and the RBM deep learning (RBM-DL) based fingerprinting algorithm [18]. The experiments is performed in the first floor lobby of the No.1 Central Building of Xi'an Jiaotong University ($length \times width = 13.2m \times 9.6m$) and the experimental system consists of 3 APs and 1 MT. Fig. 5 shows the 2-dimension layout of both the LOS experimental environment, where the 3 APs (marked red) are located in positions in a LOS with the MT, and the NLOS experimental environment where the 3 APs (marked blue) are located in positions in a NLOS with the MT at most RPs and test positions.

Considering that vector network analyzers (VNA) can provide more convenience and flexibility in measuring CSIs

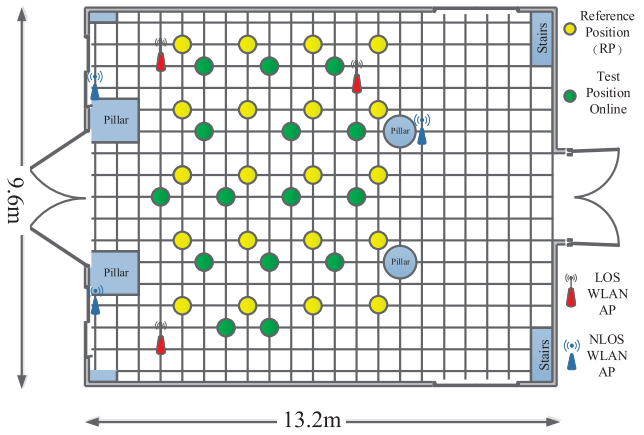

FIGURE 5. The 2-dimensional layout of the indoor experimental environment.

FIGURE 6. The virtual antenna array experimental system.

for experiments, a VNA is used to measure the indoor CFRs in the frequency range of 802.11ac: 2.4 GHz-2.48GHz, as in [11], [31]. The transmitted power of the VNA is set as 10 dBm to achieve sufficiently high SNR in the experiments, omnidirectional antennas are used as the receiving antenna and the transmitting antenna, the transmitting antenna and the receiving antenna are respectively connected to port 1 and port 2 of the VNA through two cables of length 10 m. The receiving antenna is sliding on a rail of length 1.2m to simulate the MT moving on a line trajectory, the position interval ρ is chosen as $\rho = 0.03m$ for offline and online measurements. The measurement system is shown in Fig. 6.

In the proposed method, the MT's moving direction α is discretized as $\{2\pi \cdot q/Q\}_{q=1}^{Q}$, $Q = 12$ for constructing the offline fingerprint database and the scaling factor e for the online VULA element spacing is discretized as $\mathbb{E} = \{0.8, 0.9, 1.0, 1.1, 1.2\}$. In the experiments, the offline fingerprints are collected at 20 uniformly spaced RPs with $1.8m$ spacing to build the radio map, and 30 online fingerprints at 15 test positions in two random moving directions are measured to estimate 30 MT's positions, respectively.

In the offline phase, CFRs between the MT and each AP at $M = 32$ equi-spaced positions on two trajectories perpendicular to each other with each RP as their midpoints are collected first. Based on such collected CFRs, the AOA-delay parameters of such two perpendicular moving trajectories for each RP are extracted through 2D-IFT. Further, the AOA-delay parameters of a moving trajectory with each RP as its midpoint in any direction are computed as a weighted sum of the radio fingerprints of the two perpendicular line trajectories with the same RP as their midpoints according to (7). Thus, the AOA-delay fingerprint map, including AOA-delay fingerprints in $Q = 12$ discretized directions at 30 RPs, is built up.

TABLE 1. Workload for the proposed positioning method.

	Offline workload (for each RP and each AP-MT wireless link)	**Online workload** (for each AP-MT wireless link)
Data Collection	Collecting CFRs at $M = 32$ equi-spaced positions in the X-axis and Y-axis directions	Collecting CFRs at $M = 32$ equi-spaced positions in the moving direction
Data Execution	Extracting AOA-dealy fingerprints in the X-axis and Y-axis directions: **2 2D-IFT operations**	Extracting the online AOA-dealy fingerprint: **1 2D-IFT operation**
	Constructing AOA-Delay fingerprints in Q =12 directions according to (14): **12 weighted summations**	Choosing P' nearby RPs according to the minimum path-delays in fingerprints
		Searching the minimum Euclidean distance between the online fingerprint and each nearby RP's fingerprints: $P' \times Q \times \lvert\mathbb{E}\rvert$ **Euclidean distance operations**
		Estimating the online position by WKNN: P' **weighted summations**

Similarly, the online CFRs between each AP and the MT at $M = 32$ equi-spaced positions on the moving trajectory are collected and the AOA-delay fingerprint of the moving trajectory is obtained by employing 2D-IFT on the collected CFRs in the online phase. According to the estimated minimum path-delay, the nearby RPs are then chosen. Further, the minimum Euclidean distance between the online fingerprint and each nearby RP's fingerprints with respect to the scaling factor and the Q discretized moving directions is searched. Finally, the online position is estimated as the weighted sum of the nearby RPs' position, with the weighting factor for each nearby RP proportional to the reciprocal of the minimum Euclidean distance between the online fingerprint and the nearby RP's fingerprints. For brevity, the offline workload and the online workload are summarized in Table 1.

B. POSITIONING PERFORMANCE

To show the positioning performance of the proposed algorithm, the FIFS algorithm, the CSI-MIMO algorithm and the RBM-DL algorithm, their cumulative probability distribution curves of positioning error are presented in Fig. 7. The system bandwidth is 20MHz and the number of the positions on the trajectory is 20, i.e., the VULA size is $20 \times 0.03m$, which is smaller than the length of LOS paths in experiments. It is obvious that the proposed algorithm performs better than the three existing algorithms in both the LOS environment and the NLOS environment, because the CSI or channel energy fingerprints used in the three existing fingerprinting algorithms vary rapidly in the space domain, while the proposed AOA-delay fingerprint is more robust against the variation of the spatial position due to the slow space-varying characteristics of the multipaths' delay and AOA parameters, which is illustrated in (4) and Fig. 2.

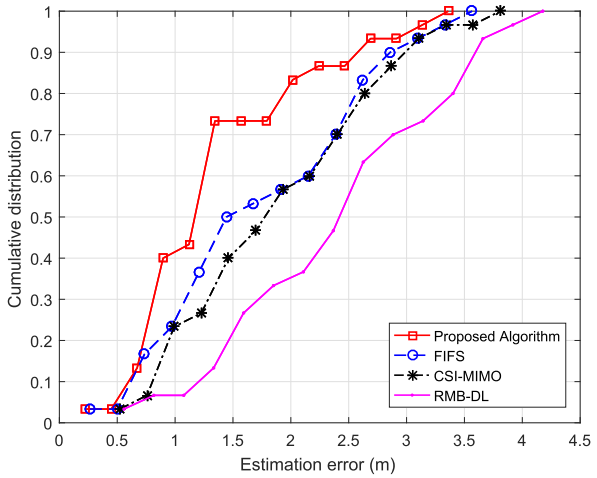

(a) LOS Environment

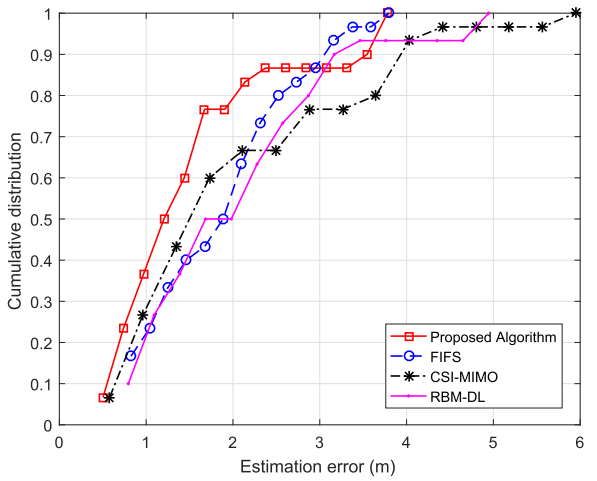

(b) NLOS Environment

FIGURE 7. The CDF of the positioning errors of the four methods in the LOS environment and NLOS environment, respectively.

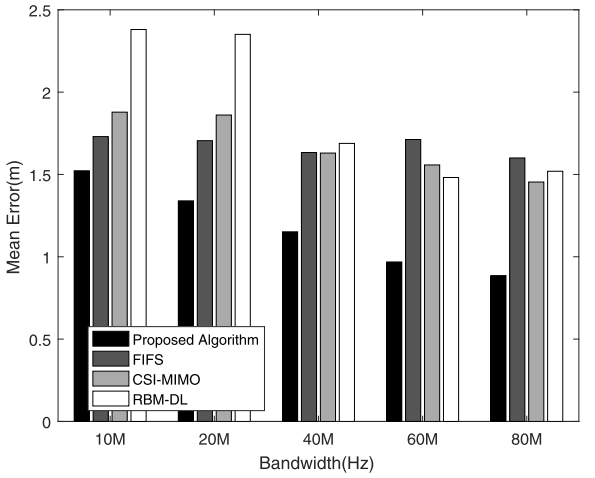

(a) LOS Environment

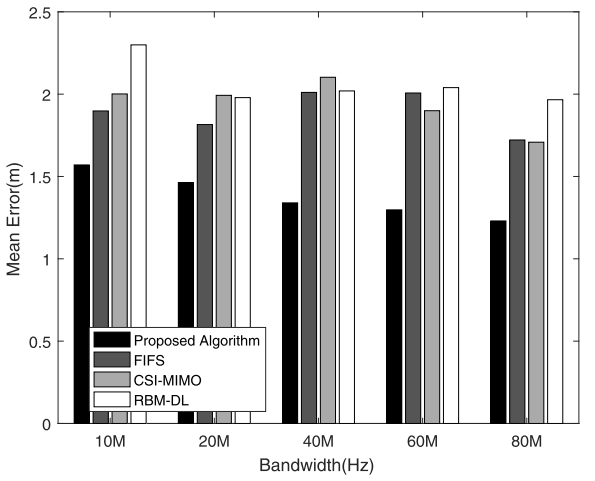

(b) NLOS Environment

FIGURE 8. Positioning performances of the four methods against different bandwidths in the LOS environment and NLOS environment, respectively.

Fig. 7 as well as Fig. 8 and Fig. 9 shows that the proposed algorithm, the FIFS algorithm and the CSI-MIMO algorithm generally perform better in the LOS environment than the NLOS environment, since the proposed algorithm suffers more from noise and interference and the FIFS algorithm and the CSI-MIMO algorithm are subject to the higher CSI fingerprints' variability over space in the NLOS environment. Besides, it has to be mentioned that the performance of the RBM-DL algorithm is worsened in cases of insufficient number of CSI samples, since the RBM-DL algorithm requires a large number of CSI samples to learn the CSI-position dependency due to the fast variation of the CSI in the space domain. This explains that the RBM-DL algorithm performs worse, even poorly, in Fig. 7, Fig. 8 and Fig. 9.

Fig. 8 shows the positioning performance of these algorithms against the system bandwidth. The number of the equi-spaced positions on the trajectory is also 20. The larger the system bandwidth is, the higher multipath resolution can be achieved and the more accurately multipaths' AOAs and delays can be estimated in the proposed method. On the other hand, the FIFS algorithm and the CSI-MIMO algorithm are mainly subject to the fast variations of the CSI and channel energy across the space dimension, and the channel stability in the space domain is hardly enhanced as the system bandwidth increases. This can explain that in Fig. 8 the performance of the proposed algorithm improves with the bandwidth increasing, while the performances of the FIFS algorithm and the CSI-MIMO algorithm slightly or barely improve with the increase of bandwidth, in both the LOS environment and the NLOS environment. Moreover, Fig. 8 shows that the performance of the RBM-DL algorithm in the LOS environment also improves with the bandwidth increasing, since more visible CSI data is input to help the RBM-DL algorithm learn the CSI-position dependency in cases of larger system bandwidth. However, the performance of the RBM-DL algorithm in the NLOS environment hardly improves with the increase of bandwidth due to the much

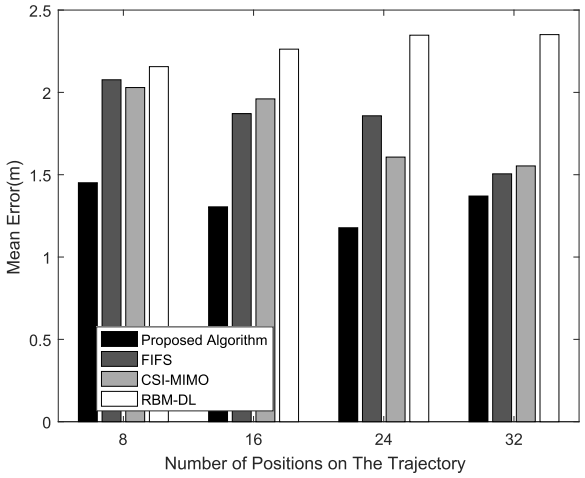

(a) LOS Environment

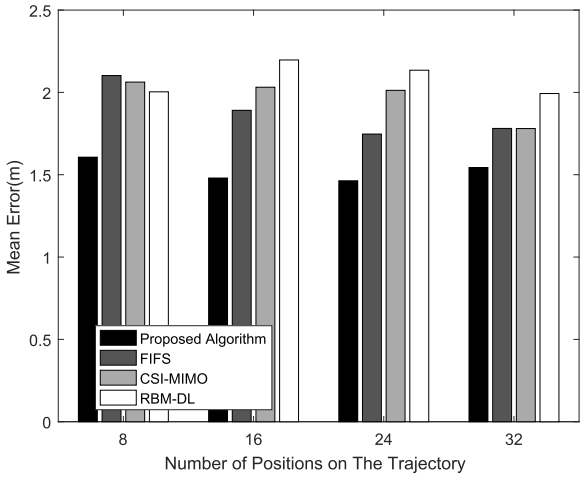

(b) NLOS Environment

FIGURE 9. Positioning performances of the four methods versus the number of positions on the line trajectory in the LOS environment and NLOS environment, respectively.

faster variation of the CSI across the space dimension in the NLOS environment.

Finally, we evaluate the positioning performances of the above algorithms against the number of positions on the line trajectory, M. The bandwidth is 20MHz and the position interval ρ is still $0.03m$. From Fig. 9, both the FIFS algorithm and the CSI-MIMO algorithm perform better with M increasing in both the LOS environment and the NLOS environment from a general view, since more test CSI samples and training samples can be used to average the channel statistics across the space dimension in the cases of larger M, thus the CSI and channel energy fingerprints can achieve higher robustness in such cases. However, the RBM-DL algorithm does not perform better with M increasing, because it suffers more seriously from insufficient samples due to the high variability of CSI.

Fig. 9 also shows that the performance of the proposed algorithm in both the LOS environment and the NLOS environment improves with the position number on the trajectory increasing in cases of relatively small position number M, while it hardly improves in cases of relatively large position number M. The reason for this phenomenon is that the higher multipath resolution can be achieved as M increases, i.e., the VULA size $M \times \rho$ increases, which means higher space 'bandwidth', on the other hand, as the position number on the trajectory M is too large, a model mismatch error is not negligible and reduces the multipath resolution. For example, $M = 32$ and the length of the trajectory $M \times \rho = 0.96m$ does not satisfy the condition $\frac{M\rho}{2c\tau_{k,l}} \ll 1$ well for (2) in the experimental scenarios.

V. DISCUSSIONS

In section II, we have adopted some ideal assumptions on the VULA system model, including the assumption of constructing a VULA by movements and the assumption of perfect frequency and timing synchronization between the MT and the AP. However, there are different timing and carrier frequency offsets at different moments and measurement errors of element spacing in forming a VULA in practice. Hence, we will briefly discuss solutions for these practical problems as follows.

A. SYNCHRONIZATION OF A VULA

Both the practical timing offset caused by packet detection delay and the carrier frequency offset (CFO) between the MT and the AP introduce additional phase shift on the measured CFRs at both the receiver (MT) and the transmitter (AP). Considering such additional phase shift, the measured CFRs at the n-th subcarrier at the k-th transmitter (AP) side and the receiver (MT) side, which is at the m-th position on the trajectory, can be expressed as

$$\hat{H}_k^{tx}(m,n) = H_k(m,n)\exp(j\phi^{tx}(m)) \cdot \exp(-j2\pi\,\Delta f n \check{\tau}^{tx}(m)) \tag{24}$$

and

$$\hat{H}_k^{rx}(m,n) = H_k(m,n)\exp(j\phi^{rx}(m)) \cdot \exp(-j2\pi\,\Delta f n \check{\tau}^{rx}(m)), \tag{25}$$

respectively, where $H_k(m,n)$ denotes the true CFR in (2), $\phi^{rx}(m)$ and $\phi^{tx}(m)$ denote the additional phase shift caused by CFO in the measured CFRs on the receiver (MT at the m-th position) and the transmitter (AP), respectively, $\check{\tau}^{rx}(m)$ and $\check{\tau}^{tx}(m)$ denote the timing offset on the receiver (MT at the m-th position) and the transmitter (AP), respectively.

Fortunately, it has been derived in [30] that such additional phase shift can be removed by multiplying the measured CFRs at the zero-subcarrier on the receiver side and the transmitter side at the same time, since the additional phase offset by CFO measured at the receiver with respect to the transmitter just changes sign when measured at the transmitter with respect to the receiver [30], and the additional phase

shift caused by timing offset is proportional to the subcarrier index.

$$\begin{aligned}&\hat{H}_k^{rx}(m,n)\cdot\hat{H}_k^{tx}(m,n)\\&\quad=H_k(m,n)\exp(j\phi^{rx}(m))\cdot H_k(m,n)\exp(-j\phi^{rx}(m))\\&\quad=(H_k(m,n))^2\end{aligned}\tag{26}$$

Therefore, by regarding the above products between CFRs at the zero-subcarriers of consecutive WiFi bands (e.g. there are 11 consecutive WiFi bands at 2.4GHz) on the receiver and the transmitter as equivalent CFRs of a VULA, the frequency and timing synchronization of the equivalent VULA system can be realized, thus the proposed multipath AOA-Delay fingerprinting method can be directly employed on such equivalent CFRs of the VULA without frequency and timing offsets.

B. CONSTRUCTING A VULA BY USING MULTIPLE ANTENNAE

In order to construct a VULA through movements, a linear moving trajectory with its distance roughly estimated as $M\rho$ is first chosen during a short period of relative small acceleration, which can be detected by built-in sensors in the MT.

Further, the multiple antennae at a WLAN AP can be optionally exploited to pick out M equi-spaced positions on the chosen moving trajectory considering the existing WLAN APs are usually equipped with more than one antenna. It can be derived that the phase difference of two CFRs between two real antennas of the AP and the MT at the central subcarrier in each WLAN frequency band varies approximately linearly across a short linear moving trajectory. Hence, the M equi-spaced positions on the trajectory can be selected according to this linear position-varying property of the phase difference between two CFRs at two real WLAN AP antennae. As the CFR phase is much more sensitive to the moving distance, the variance of the constructed array's element spacing in this VULA constructing scheme is very small, even negligible.

Therefore, a VULA with small element-spacing errors can be constructed in the proposed method by exploiting both the built-in sensors in the MT and the multiple real WLAN AP antennae.

C. PRACTICAL IMPLEMENTATION ON COMMERCIAL WiFi DEVICES

In order to prove the feasibility of the proposed method and evaluate its performance against different bandwidths, a VNA is used as the measuring device to acquire CFRs due to the fact that CFRs are unavailable on most commercial WiFi devices and the CFRs without timing and carrier frequency offsets can be acquired by the VNA, which is important for constructing the VULA. Currently, the CFRs at 30 specified subcarriers can be obtained on the off-the-shelf 802.11n device, Intel Wi-Fi Wireless Link 5300, but the acquired CFRs contain phase offset caused by the timing and carrier frequency offsets. Fortunately, the CFR phase offset correction method in [30] can be implemented on measured CFRs in such commercial WiFi devices, after modification of the firmware and the wireless driver [30]. Furthermore, both multiple antennae of WLAN APs and built-in sensors in MT can be exploited to pick out the VULA CFRs as described in section V.B. Finally, the multipath AOA-delay fingerprints can be obtained based on the corrected CFRs of the VULA and thus the multipath AOA-delay fingerprint based positioning can be realized on commercial WiFi devices.

VI. CONCLUSION

In this paper, a novel virtual antenna array based multipath fingerprinting localization algorithm was proposed. Based on the CFRs at the equi-spaced positions on a quasi-straight line moving trajectory, i.e., the CFRs of a VULA, the proposed algorithm employs 2D-IFT to extract more stable multipaths' AOAs and delays as the fingerprint. By exploiting the geometric property of the multipaths' AOAs and delays, a complete fingerprint database containing fingerprints of moving trajectories with each RP as their midpoints in different directions can be constructed from just two fingerprints of two perpendicular line moving trajectories with the same RP as the midpoints. In the online phase, the multipath delay estimates based rough location scheme was implemented to narrow the positioning scope, then a modified WKNN fingerprinting method, with the reciprocals of the fingerprints' Euclidean distances adopted as weighting factors, was further employed on the RPs in the narrowed positioning scope to enhance the positioning accuracy. Experimental evaluations in both the LOS environment and the NLOS environment confirmed that the proposed positioning algorithm can achieve better performance than the classical RSS/CSI fingerprinting methods.

APPENDIX

PROOF OF (10)

According to the geometric relationships, we have

$$\begin{aligned}x_B^2&=x_A^2sin^2\theta_l^{A,0}+d^2sin^2\gamma-2dxsin\theta_l^{A,0}sin\gamma cos\beta\\&\quad+\left(x_Acos\theta_l^{A,0}+dcos\gamma\right)^2\\&=x_A^2+d^2+2dx_A\left(cos\theta_l^{A,0}cos\gamma-sin\theta_l^{A,0}sin\gamma\cos\beta\right)\end{aligned}\tag{A.1}$$

and

$$\cos\theta_l^{B,0}=\frac{x_A\cos\theta_l^{A,0}+d\cos\gamma}{x_B}\tag{A.2}$$

From (A.1), the length of the l-th path at position B can be approximated as

$$x_B\approx x_A+d\left(\cos\theta_l^{A,0}\cos\gamma-\sin\theta_l^{A,0}\sin\gamma\cos\beta\right)\tag{A.3}$$

Further, the following approximation can be obtained from (A.2-A.3)

$$\cos\theta_l^{B,0}-\cos\theta_l^{A,0}$$

$$= \frac{d\cos\gamma - d\left(\cos\theta_l^{A,0}\cos\gamma - \sin\theta_l^{A,0}\sin\gamma\cos\beta\right)\cos\theta_l^{A,0}}{x_A + d\left(\cos\theta_l^{A,0}\cos\gamma - \sin\theta_l^{A,0}\sin\gamma\cos\beta\right)}$$
$$\approx \frac{d\left(\cos\gamma - (\cos\theta_l^{A,0}\cos\gamma - \sin\theta_l^{A,0}\sin\gamma\cos\beta)\cos\theta_l^{A,0}\right)}{x_A} \tag{A.4}$$

where the approximation holds in case of $d \ll x_A$.

It can be derived that

$$\hat{b}_l^{A,0} - \hat{b}_l^{B,0} \approx M\rho f_c(\cos\theta_l^{B,0} - \cos\theta_l^{A,0})/c \approx \frac{d\left(\cos\gamma - (\cos\theta_l^{A,0}\cos\gamma - \sin\theta_l^{A,0}\sin\gamma\cos\beta)\cos\theta_l^{A,0}\right)M\rho f_c}{x_A \cdot c} \tag{A.5}$$

$$\hat{\mathcal{T}}_l^A - \hat{\mathcal{T}}_l^B = N\Delta f\left(\tau_l^{(A)} - \tau_l^{(B)}\right) = N\Delta f d\left(\cos\theta_l^{A,0}\cos\gamma - \sin\theta_l^{A,0}\sin\gamma\cos\beta\right)/c \tag{A.6}$$

Therefore, (10) is proved.

REFERENCES

[1] H. Zou, B. Huang, X. Lu, H. Jiang, and L. Xie, "A robust indoor positioning system based on the procrustes analysis and weighted extreme learning machine," *IEEE Trans. Wireless Commun.*, vol. 15, no. 2, pp. 1252–1266, Feb. 2016.
[2] R. Liu, C. Yuen, T.-N. Do, M. Zhang, Y. L. Guan, and U.-X. Tan, "Cooperative positioning for emergency responders using self IMU and peer-to-peer radios measurements," *Inf. Fusion*, vol. 56, pp. 93–102, Apr. 2020.
[3] A. Yassin, Y. Nasser, M. Awad, A. Al-Dubai, R. Liu, C. Yuen, R. Raulefs, and E. Aboutanios, "Recent advances in indoor localization: A survey on theoretical approaches and applications," *IEEE Commun. Surveys Tuts.*, vol. 19, no. 2, pp. 1327–1346, 2nd Quart., 2017.
[4] C. Yang and H.-R. Shao, "WiFi-based indoor positioning," *IEEE Commun. Mag.*, vol. 53, no. 3, pp. 150–157, Mar. 2015.
[5] C. Feng, W. S. A. Au, S. Valaee, and Z. Tan, "Received-signal-strength-based indoor positioning using compressive sensing," *IEEE Trans. Mobile Comput.*, vol. 11, no. 12, pp. 1983–1993, Dec. 2012.
[6] S.-H. Fang and T. Lin, "Principal component localization in indoor WLAN environments," *IEEE Trans. Mobile Comput.*, vol. 11, no. 1, pp. 100–110, Jan. 2012.
[7] Z. Yang, Z. Zhou, and Y. Liu, "From RSSI to CSI: Indoor localization via channel response," *ACM Comput. Surv.*, vol. 46, no. 2, pp. 25:1–25:32, Dec. 2013.
[8] Y. Xie, Y. Wang, P. Zhu, and X. You, "Grid-search-based hybrid TOA/AOA location techniques for NLOS environments," *IEEE Commun. Lett.*, vol. 13, no. 4, pp. 254–256, Apr. 2009.
[9] X. Li and K. Pahlavan, "Super-resolution TOA estimation with diversity for indoor geolocation," *IEEE Trans. Wireless Commun.*, vol. 3, no. 1, pp. 224–234, Jan. 2004.
[10] T. K. Sarkar and O. Pereira, "Using the matrix pencil method to estimate the parameters of a sum of complex exponentials," *IEEE Antennas Propag. Mag.*, vol. 37, no. 1, pp. 48–55, Feb. 1995.
[11] A. Gaber and A. Omar, "A study of wireless indoor positioning based on joint TDOA and DOA estimation using 2-D matrix pencil algorithms and IEEE 802.11ac," *IEEE Trans. Wireless Commun.*, vol. 14, no. 5, pp. 2440–2454, May 2015.
[12] J. M. Huerta, J. Vidal, A. Giremus, and J.-Y. Tourneret, "Joint particle filter and UKF position tracking in severe non-line-of-sight situations," *IEEE J. Sel. Topics Signal Process.*, vol. 3, no. 5, pp. 874–888, Oct. 2009.
[13] D. E. Gustafson, M. S. Bottkol, J. R. Parry, J. M. Elwell, and T. Q. Nguyen, "Indoor geolocation using RF multipath with probabilistic data association," in *Proc. IEEE/ION Position, Location Navigat. Symp.*, May 2008, pp. 402–412.
[14] J. Ma, X. Li, X. Tao, and J. Lu, "Cluster filtered KNN: A WLAN-based indoor positioning scheme," in *Proc. Int. Symp. World Wireless, Mobile Multimedia Netw.*, Jun. 2008, pp. 1–8.
[15] C. Chen, Y. Chen, Y. Han, H.-Q. Lai, and K. R. Liu, "Achieving centimeter-accuracy indoor localization on WiFi platforms: A frequency hopping approach," *IEEE Internet Things J.*, vol. 4, no. 1, pp. 111–121, Feb. 2017.
[16] G. I. Wassi, C. Despins, D. Grenier, and C. Nerguizian, "Indoor location using received signal strength of IEEE 802.11b access point," in *Proc. Can. Conf. Electr. Comput. Eng.*, 2005, pp. 1367–1370.
[17] Y.-P. Lin, P.-H. Tseng, and K.-T. Feng, "Compressive sensing based location estimation using channel impulse response measurements," in *Proc. IEEE 25th Annu. Int. Symp. Pers., Indoor, Mobile Radio Commun. (PIMRC)*, Sep. 2014, pp. 2066–2070.
[18] X. Wang, L. Gao, S. Mao, and S. Pandey, "CSI-based fingerprinting for indoor localization: A deep learning approach," *IEEE Trans. Veh. Technol.*, vol. 66, no. 1, pp. 763–776, Jan. 2017.
[19] A. Kushki, K. N. Plataniotis, and A. N. Venetsanopoulos, "Kernel-based positioning in wireless local area networks," *IEEE Trans. Mobile Comput.*, vol. 6, no. 6, pp. 689–705, Jun. 2007.
[20] X. Wang, L. Gao, and S. Mao, "CSI phase fingerprinting for indoor localization with a deep learning approach," *IEEE Internet Things J.*, vol. 3, no. 6, pp. 1113–1123, Dec. 2016.
[21] J. Xiao, K. Wu, Y. Yi, and L. M. Ni, "FIFS: Fine-grained indoor fingerprinting system," in *Proc. 21st Int. Conf. Comput. Commun. Netw. (ICCCN)*, Jul./Aug. 2012, pp. 1–7.
[22] Y. Chapre, A. Ignjatovic, A. Seneviratne, and S. Jha, "CSI-MIMO: Indoor Wi-Fi fingerprinting system," in *Proc. 39th Annu. IEEE Conf. Local Comput. Netw.*, Sep. 2014, pp. 202–209.
[23] X. Sun, X. Gao, G. Y. Li, and W. Han, "Single-site localization based on a new type of fingerprint for massive MIMO-OFDM systems," *IEEE Trans. Veh. Technol.*, vol. 67, no. 7, pp. 6134–6145, Jul. 2018.
[24] X. Sun, X. Gao, G. Y. Li, and W. Han, "Fingerprint based single-site localization for massive MIMO-OFDM systems," in *Proc. IEEE Global Commun. Conf. (GLOBECOM)*, Dec. 2017, pp. 1–7.
[25] A. Jaffe and M. Wax, "Single-site localization via maximum discrimination multipath fingerprinting," *IEEE Trans. Signal Process.*, vol. 62, no. 7, pp. 1718–1728, Apr. 2014.
[26] E. Kupershtein, M. Wax, and I. Cohen, "Single-site emitter localization via multipath fingerprinting," *IEEE Trans. Signal Process.*, vol. 61, no. 1, pp. 10–21, Jan. 2013.
[27] S. Feng and R. Murray-Smith, "Fusing kinect sensor and inertial sensors with multi-rate Kalman filter," in *Proc. IET Conf. Data Fusion Target Tracking, Algorithms Appl.*, 2014, vol. 10, no. 3, pp. 1–8.
[28] W. Kang and Y. Han, "SmartPDR: Smartphone-based pedestrian dead reckoning for indoor localization," *IEEE Sensors J.*, vol. 15, no. 5, pp. 2906–2916, May 2015.
[29] M. C. Vandeveen, A. J. Van der Veen, and A. Paulraj, "Estimation of multipath parameters in wireless communications," *IEEE Trans. Signal Process.*, vol. 46, no. 3, pp. 682–690, Mar. 1998.
[30] D. Vasisht, S. Kumar, and D. Katabi, "Decimeter-level localization with a single WiFi access point," in *Proc. 13th USENIX Symp. Netw. Syst. Design Implement. (NSDI)*, Mar. 2016, pp. 165–178.
[31] N. A. Alsindi, B. Alavi, and K. Pahlavan, "Measurement and modeling of ultrawideband TOA-based ranging in indoor multipath environments," *IEEE Trans. Veh. Technol.*, vol. 58, no. 3, pp. 1046–1058, Mar. 2009.

ZHIGANG CHEN (Member, IEEE) received the B.S. and M.S. degrees from Northwestern Polytechnical University, Xi'an, China, in 1998 and 2001, respectively, and the Ph.D. degree from Xi'an Jiaotong University, Xi'an, in 2006. From September 2006 to December 2008, he worked as a Research Scientist with Philips Research Asia-Shanghai, Shanghai, China. He is currently an Associate Professor with Xi'an Jiaotong University. His research interests include wireless positioning technology and massive MIMO technology.

LEI WANG received the Ph.D. degree from Xi'an Jiaotong University, Xi'an, China, in 2006. From December 2006 to March 2008, she worked as a Research Engineer with the Research and Innovation Center, Alcatel-Lucent, Shanghai. From October 2016 to September 2017, she worked as a Visiting Scholar with the University of Delaware, USA. She is currently an Associate Professor with Xi'an Jiaotong University. Her research interests include MIMO systems, space-time signal processing, and cooperative communications.

LU CHEN was born in China, in 1996. He received the B.S. degree in information and communication engineering from Xi'an Jiaotong University, Xi'an, China, in 2018, where he is currently pursuing the M.S. degree with the School of Information and Communication Engineering. His research interest includes wireless positioning technology.